The Effect of Hatch Angle Rotation on Parts Manufactured using Selective Laser Melting

Abstract

Purpose

This paper presents an investigation into the variation of scan vector hatch rotation strategies in selective laser melting (SLM) focusing on how this effects density, surface roughness, tensile strength and residual stress.

Design/methodology/approach

First the optimum angle of hatch vector rotation is proposed by analysing the effect of different increment angles on distribution of scan vectors. Sectioning methods are then used to determine the effect that the chosen strategies have on the density of the parts. The top surface roughness was analysed using optical metrology and the tensile properties were determined using uni-axial tensile testing. Finally a novel multi-support deflection geometry was used to quantify the effects of rotation angles on residual stress.

Findings

The results of this research showed that the hatch rotation angle had little effect on the density, top surface roughness and strength of the parts. The greatest residual stress deflection was measured parallel to unidirectional scan vectors. The use of hatch rotations other than alternating 90° showed little benefit in lowering the magnitude of residual stresses. However the use of rotation angles with a good suitability measure distributes stresses in all directions more evenly for certain part geometries.

Research limitations/implications (if applicable)

All samples produced in this work were made from Commercially Pure Titanium therefore care must be taken when applying these results to other materials.

Originality/value

This paper serves to increase the understanding of SLM scanning strategies and their effect on the properties of the material.

Article Classification
Research Paper

Keywords (max 10)

Selective Laser Melting, Laser Powder Bed Fusion, Residual Stress, Tensile Strength, Hatch Rotation, Roughness, Density

Introduction

Selective laser melting (SLM) is an additive manufacturing (AM) technology, which creates fully dense metal parts from fine metal powders. Over the last 15 years, technological developments have enabled the transition from a prototyping technology to a manufacturing technology that can be used for one off, batch or mass production. The material properties of the metals produced by this process have been shown to be similar and in some cases exceed that of the expected values quoted in the relevant standards, with little or no requirement for post process treatments (Mullen et al. 2009).

The SLM technology is a powder bed based additive manufacturing technique where, 20 to 150 µm thick, layers of powder build material are successively laid upon a substrate of a similar material. After the deposition of each layer a high power laser, 50W to 1kW, is used to selectively melt the metal powder and underlying material to ensure metallurgical bonding. The area melted is defined by a 3D CAD model of the desired part which is sliced into layers of corresponding thickness to the powder layer to produce slice data. The area of the slice that is designated to be solid is then exposed to the laser beam in a pattern defined by a hatch strategy. The hatch strategy of an individual layer consists of a raster pattern of scan vectors which fill the internal geometry. Commonly the direction of each subsequent scan vector is rotated by 180° forming an orthogonal pattern across the part (Figure 1). This area fill scan is then followed by a boundary scan vector of differing process parameters at the edge of the layer to improve the outer surface finish. On creation of the subsequent layer the direction of the scan vectors are generally rotated by a set hatch rotation angle, ϕ. The most common embodiment of this being 90° also denoted as XY alternating (XYA). After the completion of all the build layers the unfused powder is removed, sieved and returned to the AM machine or storage for reuse.

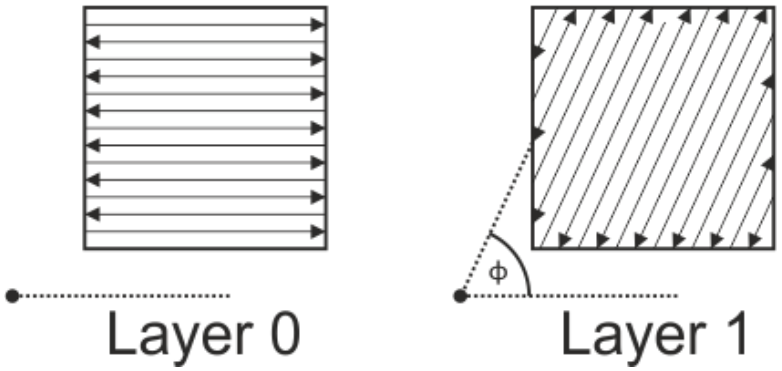

Figure 1 Simple scan strategy with raster scanning in the layers and a rotation of the vectors by the angle ϕ for subsequent layers.

Over the last 15 years many developments and improvements to the SLM process have been made however, many problems still exist. Chief amongst these issues are the high thermal gradients which are a consequence of the rapid melting and cooling of the material as it is processed. These gradients cause thermal stresses within the parts (Shiomi et al. 2004; Mercelis & Kruth 2006) which remain in the part after manufacture and can cause built parts to deform or cracks to propagate in service. Despite many discussed and implemented developments these stresses can be a significant issue dependent on the size and shape complexity of the component being produced. Previous work has shown that the choice of scanning strategy has a significant effect on the magnitude and direction of

these stress (Kruth et al. 2010; Mercelis & Kruth 2006). The primary direction of residual stress with respect to the direction of the scan vectors has been much debated with early studies proposing the greatest stress is generated orthogonally to the scan vectors (Pohl et al. 2001; Kruth et al. 2004; Mercelis & Kruth 2006) and later studies indicating that they are parallel to the scan vectors (Kruth et al. 2010). Clearly this dichotomy needs further in-depth investigation to arrive at a satisfactory conclusion.

The proposed mechanism for the development of the residual stress is a combination of the thermal gradient mechanism (TGM) and the constrained contraction of material on cooling (Shiomi et al. 2004; Mercelis & Kruth 2006) . The TGM generates stresses in already deposited solid material below the melt pool, because as this material heats up it expands but is constrained by the surrounding solid; this causes the heated material to yield. On cooling the compressed zone formed is effectively shorter than it was before which causes tensile stresses to be created in the top of the part. The constrained contraction mechanism occurs because of the thermal gradients following solidification. Owing to the steep thermal gradients there is a mismatch in the shrinkage on cooling creating tensile stresses in the upper region of the part.

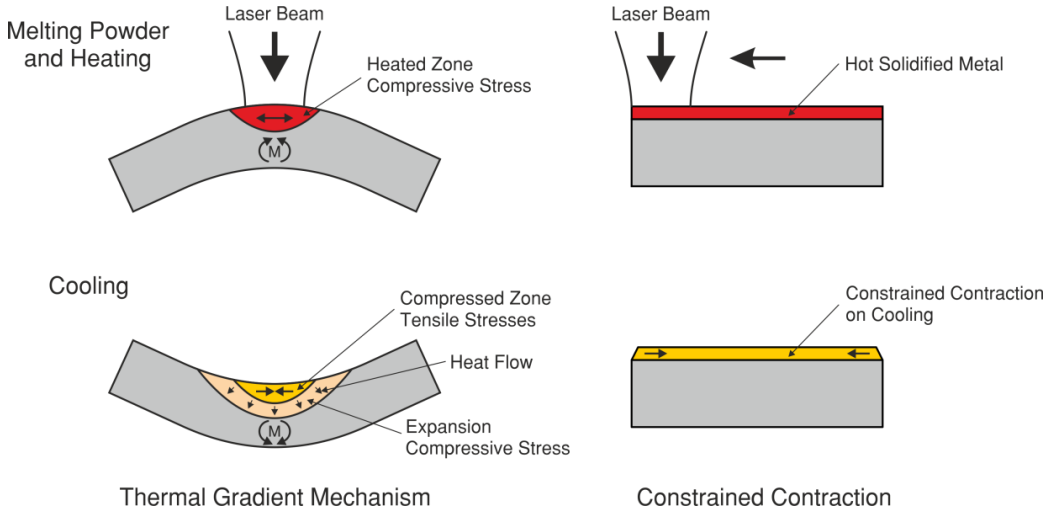

Figure 2 Mechanisms that contribute to the residual stresses in parts manufactured using SLM (adapted from (Vollersten 1998) **and** (Shiomi et al. 2004)**).**

The surface finish and anisotropy of the material properties caused by layer-wise manufacture also affects downstream process that may be required to produce a functional part. For example, high residual stress might result in the requirement for lengthy post manufacture heat treatment or the addition of considerable amounts of machining stock on parts. It has been proposed that the need for post processing can be reduced by the rotation of scan vectors on successive layers at an angle of 67°. This angle has been reported to reduce anisotropy, warping, and the number of defects and surface roughness of the finished item. The 67° rotation was proposed as it was believed that at this value the scan vector direction would not repeat (to within 10° error) for the maximum number of layers (Dimter et al. 2011). Guan et al. (2013) indicated that small increases in the strength of 304 Stainless steel were achievable with hatch rotations of 105°. Kruth (2012) performed a short study showing that residual stress could be reduced as the initial hatch angle was varied. However the actual rotation between each layer was fixed at 90° therefore only hatch vector length and part orientation was actually being investigated. Other studies which include hatch angle rotation variations, such as

several studies by Thijs (2010; 2013), have concentrated on 0°, 60°and 90° rotations only and concentrated on density and microstructure.

Although 67° and 105° have been reported to be more suitable rotation angles in comparison to 90° there are many others that are possible. This paper aims to evaluate the real effect of hatch rotation angle on the SLM process in order to provide insight into how future scan strategies may be developed to minimise in-built stresses and the detrimental effect they may have on component quality.

Theory

In order to assess the current status with respect to hatch rotation one must first consider carefully the effect of rotation and how it may be optimised. In this section the accumulative effect of additional layers to hatch distribution will be discussed and a hatch angle criterion is developed.

To determine the optimum hatch rotation angle, the number of layers until the vector direction repeated within 10° of the initial vector direction was calculated with the following assumptions:

- Only integer values are considered.
- Hatch vectors will follow a raster pattern i.e. subsequent vectors will have a rotation of 180° resulting in a direction change.
- The maximum hatch angle rotation is 90°. Any rotation angle above this can be considered to be equal to 180° - ϕ and therefore an acute angle, rotating in the opposite direction.
- Due to the above assumption any angles ≥ to 180 ° will be converted to their obtuse or acute equivalent.
- When calculating the angle between scan vectors the smallest angle will be chosen i.e. acute angles are forced.

The resulting repeat characteristics for a full range of hatch rotation angles is shown in Figure 3.

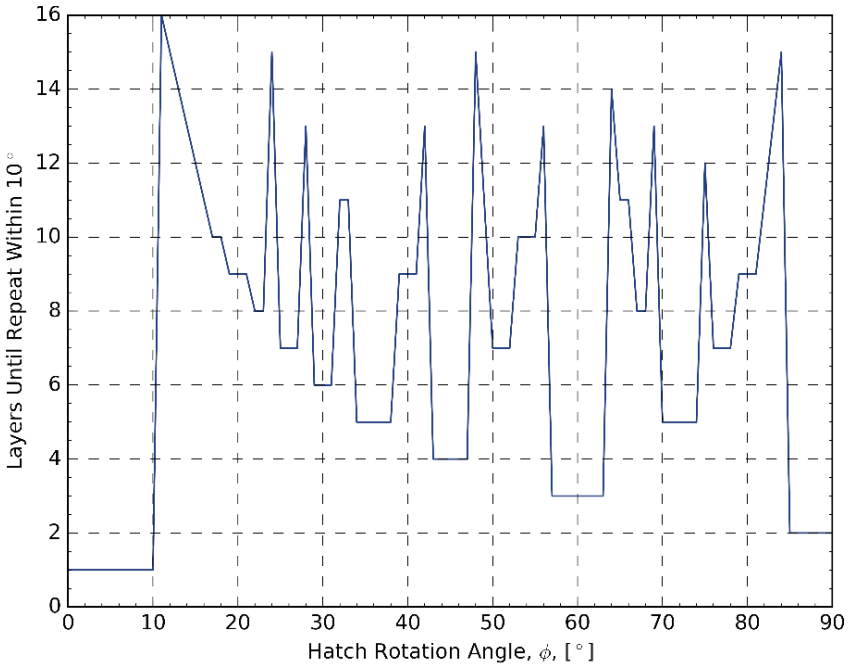

Figure 3 Number of layers before the scan vector direction repeats within 10° of the initial direction.

Whilst Dimter (2011) cites 67° as being the optimum as it takes 18 layers repeat within 10° this observation changes if the assumption that a raster pattern of alternating vectors is used. The number of layers until the 67° scan strategy returns to within 10° of the initial vector is reduced to 8. Figure 3 shows that the neighbouring rotation increments of 64° and 69° increase the number of layers until angular repeat, within 10° of the initial direction, to 14 and 13 layer respectively.

The number of layers until repeat is only a part of the picture as it does not help to understand the distribution of vectors over the layers. A method that could be used to better describe the distribution is as follows:

1. Calculate the rotation angle of all vectors over n layers.
2. Determine the angular increments between adjacent hatch angles regardless of layer number (Figure 4).
3. Determine the standard deviation of these angular increments.

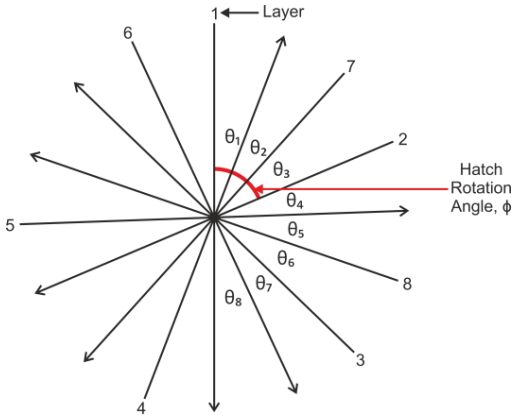

Figure 4 Distribution of angular increments, θ, between closest hatch rotations regardless of layer number.

An evenly distributed pattern would result in a small standard deviation measurement of the angular increments. However this measurement only describes the distribution after n layers and not how the distribution has developed with each additional layer. Consider a hatch rotation angle of 10° (Figure 5), initially the vector distribution looks poor due to the small angular step and therefore results in a large deviation. However after many layers the distribution is very even and returns a low standard deviation. The distribution measure is therefore strongly biased by the number of layers being considered.

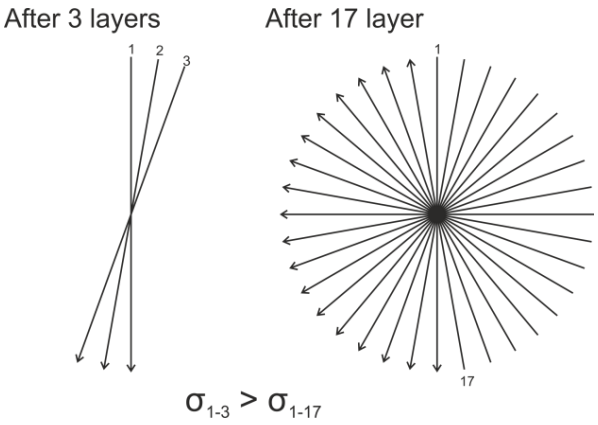

Figure 5 Hatch distribution for a 10° angular step after 3 and 17 layers.

A measure of how the vector distribution developed was determined by calculating the standard deviation of adjacent angular increments after the addition of each new layer, i.e. $\sigma_{layer\ 1\text{-}2}$, $\sigma_{layer\ 1\text{-}3}$, … $\sigma_{layer\ 1\text{-}n}$. This provides a list of measurements that record the progression in the vector distribution as new layers are added. By taking the combined standard deviation of these deviation measurements an insight into how the vector distribution develops can be made. It was theorised that a hatch rotation angle which consistently produced an evenly distributed vector pattern would be beneficial for reducing or distributing residual stress; this would be identified by a low standard deviation of the combined layer deviations.

However, there was an issue with the combined standard deviation at hatch rotation angles which rapidly repeated, such as 45°, 60° and 90°. These angles consistently return large deviations and therefore on calculation of the combined deviation measurement a low value is returned. This incorrectly suggests that the selected hatch rotation angles evenly distributed hatch vectors throughout manufactured components. A Suitability Measure, M, was therefore defined as the mean layer standard deviation multiplied by the combined deviation. Patterns with poor repeating distributions resulted in large mean values and therefore returned large suitability measures. The goal was to find hatch rotation angles with a low Suitability Measurement as these would results in consistently distributed vector patterns. The process to calculate the Suitability Measure for a given hatch rotation angle is described below.

- Calculate the angle between adjacent hatch vectors, θ, after k layers for a given hatch rotation angle, ϕ

$$Adjacent\ angle\ list = \begin{vmatrix} \theta_1 \\ \theta_2 \\ \dots \\ \theta_k \end{vmatrix}$$

- Calculate the individual standard deviation

$$\sigma_{1\to k} = \sqrt{\frac{1}{k}\sum_{i=1}^{k}(\theta_i - \bar{\theta})^2}$$

- Repeat for all additional layers from $k = 2 \rightarrow n$

$$Standard\ deviation\ list = \begin{vmatrix} \sigma_{1\to 2} \\ \sigma_{1\to 3} \\ \dots \\ \sigma_{1\to n} \end{vmatrix}$$

- Calculate the combined standard deviation

$$\sigma_{Combined} = Standard\ Deviation \begin{vmatrix} \sigma_{1\to 2} \\ \sigma_{1\to 3} \\ \dots \\ \sigma_{1\to n} \end{vmatrix}$$

- Calculate the combined mean

$$\bar{\sigma} = Mean \begin{vmatrix} \sigma_{1\to 2} \\ \sigma_{1\to 3} \\ \dots \\ \sigma_{1\to n} \end{vmatrix}$$

- Calculate the Suitability Measure for the hatch rotation angle

$$M_{\emptyset} = \bar{\sigma} \cdot \sigma_{Combined}$$

From the Suitability Measure for integer hatch rotation angles from 1° to 90° after 180 layers (Figure 6) it can be seen that the strategies that repeat quickly, 45°, 60°and 90°, all show a peak on the graph denoting that they do not give an even distribution of scan vectors.

Eighteen different scanning strategies were chosen to be tested. Unidirectional scan vectors in the X, Y and at 45°, a rotation of 90° on subsequent layers starting at both 0° and 45°, rotations of 60° and 45° were chosen as these repeat after 3 and 4 layers respectively. As 67° has been promoted as the

optimum scan angle this was also tested. As well as the conventional rotations chosen the angles of 41°, 69°, 74° ,76° and 79° were chosen as these all had both a high number of layers until repeat with in 10° and a good distribution of scan vectors as determined from the Suitability Measure.

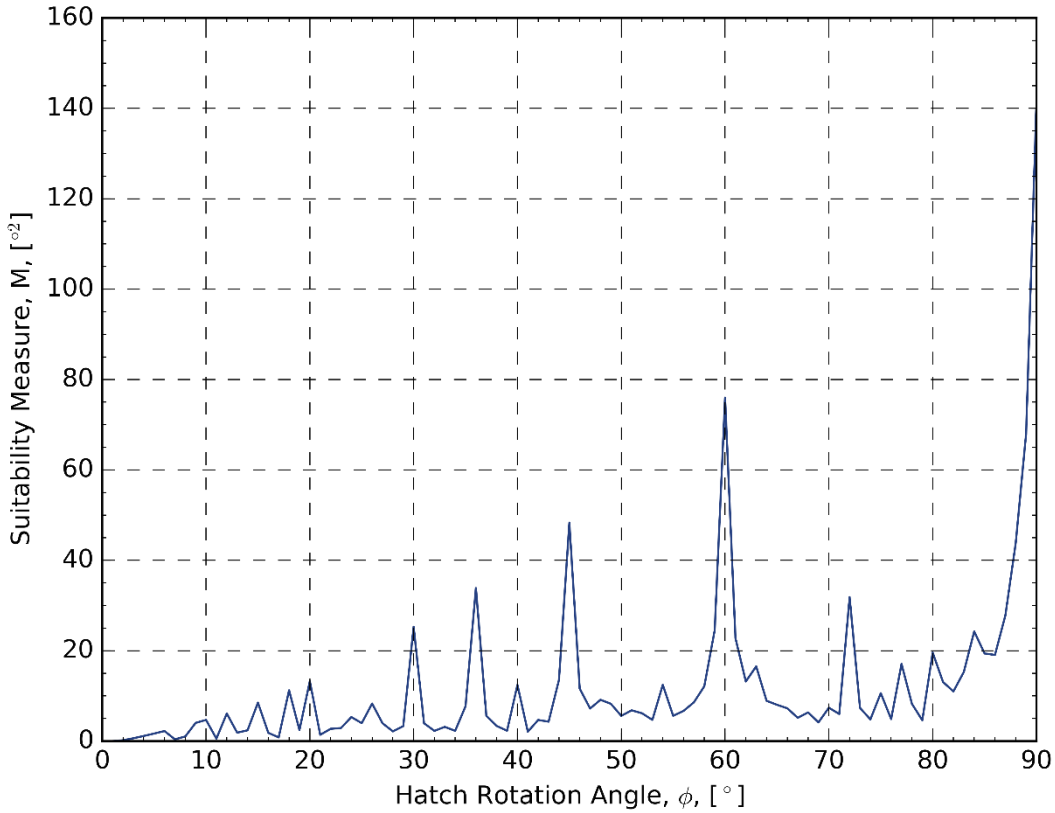

Figure 6 Measure of the distribution of scan vectors over 2 to 180 layers.

To determine the sensitivity of the process to the value of hatch angle rotation a further five strategies were chosen. Four of the test samples had a small degree of randomisation added to the increment angle between subsequent scan layers. This method employed a Gaussian randomisation function to determine the angle of increment. The function was provided with the position of the centre of the Gaussian distribution in this case either 60° or 74° and then the standard deviation for the Gaussian curve of either 5° or 10°. The final strategy was one that was fully random, this was achieved with a Gaussian centre of 90° and a standard deviation of 180°. A summary of all test hatch rotation angles are shown in Table 1.

Table 1 Summary of the selected test hatch angle rotations.

Test Identifier	Initial hatch angle	Hatch rotation angle	Suitability Measure, M	Density Sample Locations
All X	0°	0°	NA	O-11, P-11
All 45°	45°	0°	NA	O-09, P-04
All Y	90°	0°	NA	P-05, U-05
XYA	0°	90°	99.6	O-08, U-03
45 XYA	45°	90°	99.6	O-10, U-04
60° inc	0°	60°	44.3	O-02, U-00
41° inc	0°	41°	1.0	O-00, U-11

45° inc	0°	45°	35.4	O-01, P-00
67° inc	0°	67°	2.0	O-03, P-01
69° inc	0°	69°	1.9	O-04, U-01
74° inc	0°	74°	2.1	O-05, P-02
76° inc	0°	76°	2.4	O-06, U-02
79° inc	0°	79°	2.0	O-07, P-03
60° -5° sigma	0°	$60° \pm 5°$	Variable	P-06, U-06
60° -10° sigma	0°	$60° \pm 10°$	Variable	P-07, U-07
74° -5° sigma	0°	$74° \pm 5°$	Variable	P-08, U-08
74° -10° sigma	0°	$74° \pm 10°$	Variable	P-09, U-09
Random	0°	0° – 90°	Variable	P-10, U-10

Experimental Methods

All samples were built with the same parameters on a Realizer II SLM250 (Realizer, Germany) in grade 1 commercially pure titanium (CpTi) powder TILOP (Sumitomo, Japan) using the parameters shown in Table 2.

Table 2 Process parameters for the Realizer SLM250 for CpTi.

Parameter	Hatch Vectors	Boundary Scan
Power [W]	180	100
Exposure Time [µs]	50	300
Point Distance [µm]	70	65
Hatch Distance [µm]	100	N/A
Hatch Offset [µm]	50	N/A
Slice Thickness [µm]	50	50
Focal Beam Diameter [µm]	73	52

To evaluate the bulk density, sets of density cuboids, 5 mm sides by 10 mm tall, were manufactured on a support tower. Each of which held 12 individual samples as shown in Figure 7a. Each hatch strategy was manufactured twice and therefore 36 samples were distributed over three support towers. The locations of each strategy are displayed in Table 1 and related to physical positions using Figure 7b and Figure 7c. Following production the top 1 mm of each coupon was removed using an Isomet 4000 (Buehler, USA) precision saw and the whole sample set vacuum mounted in epoxy resin and polished to a finish of 40 nm using standard metallographic techniques. Each sample was imaged at 5 separate bulk solid locations at 25x magnification with an optical microscope. The edges of each sample were deliberately avoided as not to include sub-surface porosity due to the non-optimised boundary scan parameters for each hatch rotation strategy. Each sample image was converted to an 8-bit grey scale image and then converted to a binary image with a threshold value of 100, this isolated pores from bulk material. The fraction of the image define as bulk material was used as the density value.

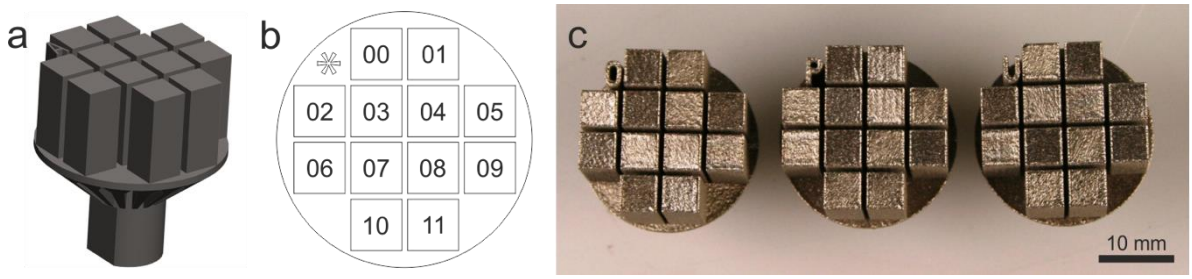

Figure 7 Density evaluation samples for the hatch angle tests. a) CAD representation of a complete density tower b) sample locations on each tower c) Image of the unprocessed density towers labelled O, P and U.

The top surface profile was measured using the OSP100 (Uniscan, UK) laser triangulation surface profiler, 10 mm cubes were built directly onto the substrate plate and an 8 mm square was profiled in the centre of each cube. Measurements were taken on a grid spacing of 10 µm by 50 µm. Two samples for each scanning strategy were built and the surface roughness (Ra) was calculated for each. The side surface roughness of the samples were not measured during this study. The hatch rotation directly effects the top surface roughness, however the side surface roughness is determined by the boundary scan and these parameters were not varied though this study. As a result side surface finish remained consistent across the sample set.

The effect of hatch strategy on the strength of the samples was determined by uni-axial tensile testing using the sample geometry according to the ISO 6892 standard (Figure 8). The test specimen were built in the z axis such that the gauge cross section laid in the XY plane. Under testing the applied tension therefore aligned with the machine build axis. The 18 test strategies were reduced to 15 by removing strategies with identical hatch rotation increments. As the cross section of the tensile specimens was small (6 mm x 6 mm), little variation of hatch vector lengths occurred between samples with different initial hatch angles and therefore identical strengths would be recorded. As a result strategies All X, All 45°, and All Y were replaced by All X only along with XYA and XYA 45° being replaced by XYA only. Three copies of each test strategy were built on a single build plate, the locations of each tensile specimen was randomised to eliminate any positional bias of the machine. The specimens were tested on a universal tensile testing machine with a 12.5mm gauge length extensometer (Instron, USA) at room temperature using a cross-head speed of 1 mm/min. The external surfaces of the samples were rubbed down with 240 grit paper to create a smooth sample surface. This was performed to reduce the possibility of increased notch sensitivity of the samples due to the side surface finish. This would resulted in a reduction in likelihood of premature sample failure affecting elongation to failure measurements.

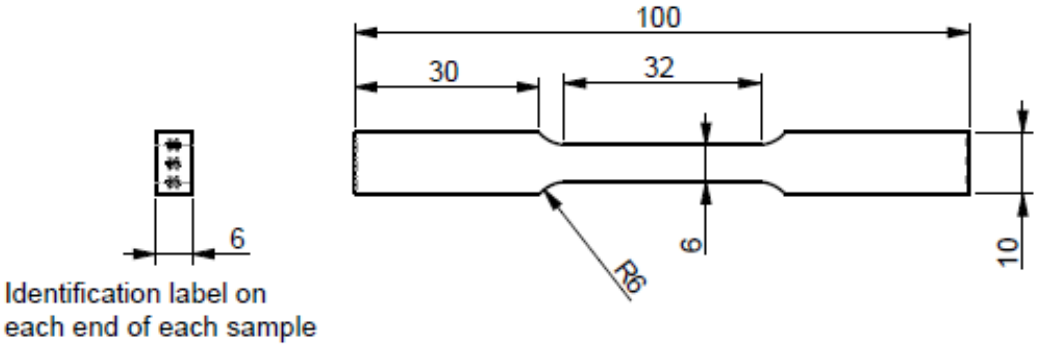

Figure 8 Geometry of the tensile test specimens (dimensions in mm).

Residual stress levels were determined using a novel multi-support deflection bridge (MSDB) geometry. Comparison between different strategies is made from the deflection of the top surface of a test part when released from the substrate (Figure 9) in a similar manner to Pohl (2001) and Kruth et al. (2010). The length to width aspect ratio of the test samples was > 5:1 to prevent multiaxial curvature (Withers & Bhadeshia 2001). This feature isolated the majority of the residual stress into the largest dimension of the sample and therefore hatch rotation angle could be assessed with greater accuracy. The parts were cut from the substrate using a band saw and the top surface was profiled using the OSP100. Three test samples for each hatch rotation were built with the parts being randomised across the build plate to remove any systematic errors caused by differences in properties across the build area (Hague et al. 2004).

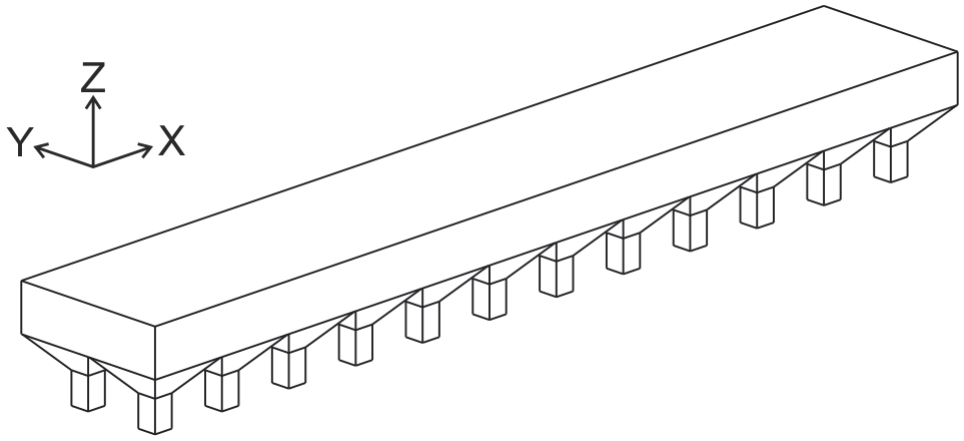

Figure 9 Residual stress MSDB consisting of a 60 mm x 10 mm x 3 mm beam supported on 5 mm pyramid structures.

Results and Discussion

Density Characteristics

The effect of hatch rotation on the density of the parts is shown in Figure 10. The angle of rotation appears to have little effect with all the samples having an average density greater than 99.95%. This suggests that the density is independent of the angle of rotation and based more on the material parameters used to make the solid. The material build parameters had been extensively tested in order to achieve high density (>99.95%) with an XY alternating hatch pattern. The result demonstrates that the density is not sensitive to hatch rotation for non-optimised process parameters. This agrees with simulation studies presented by Tang (2017) into part porosity derived from variations in hatch angle rotation.

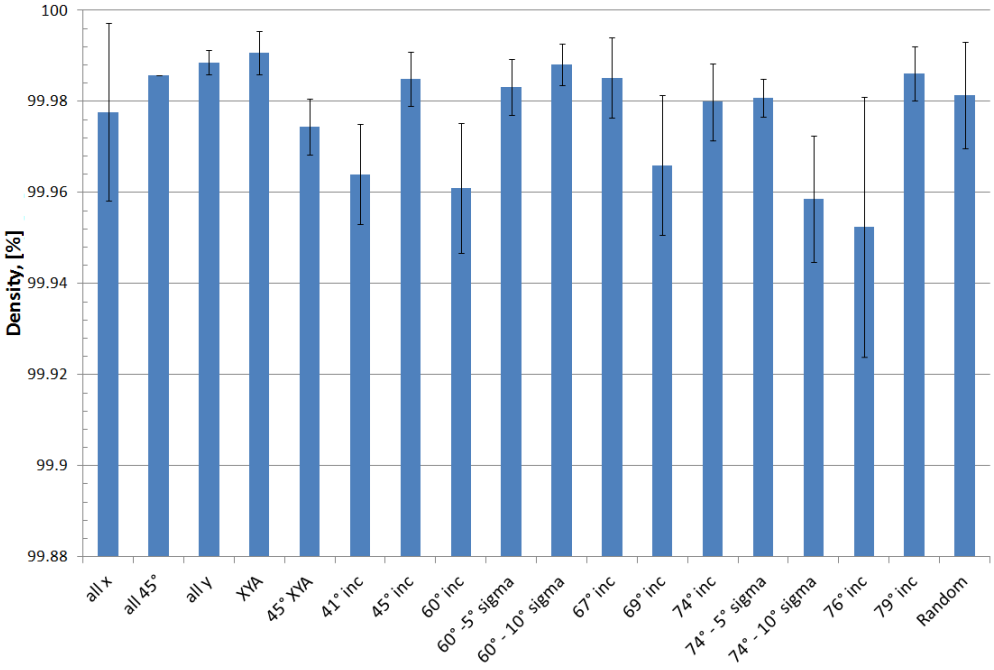

Figure 10 Density of the samples produced with different hatch rotations determined by metallography.

Surface Finish Characteristics

The top surface finish of the samples is similar for all the samples built (Figure 11). With a roughness value of 10 µm Ra for all samples with the exception of the all X and the all Y axis raster scan patterns. These are slightly rougher because the scan vectors line up on subsequent layers thereby allowing the possibility for troughs to form resulting in a consequential increase in roughness.

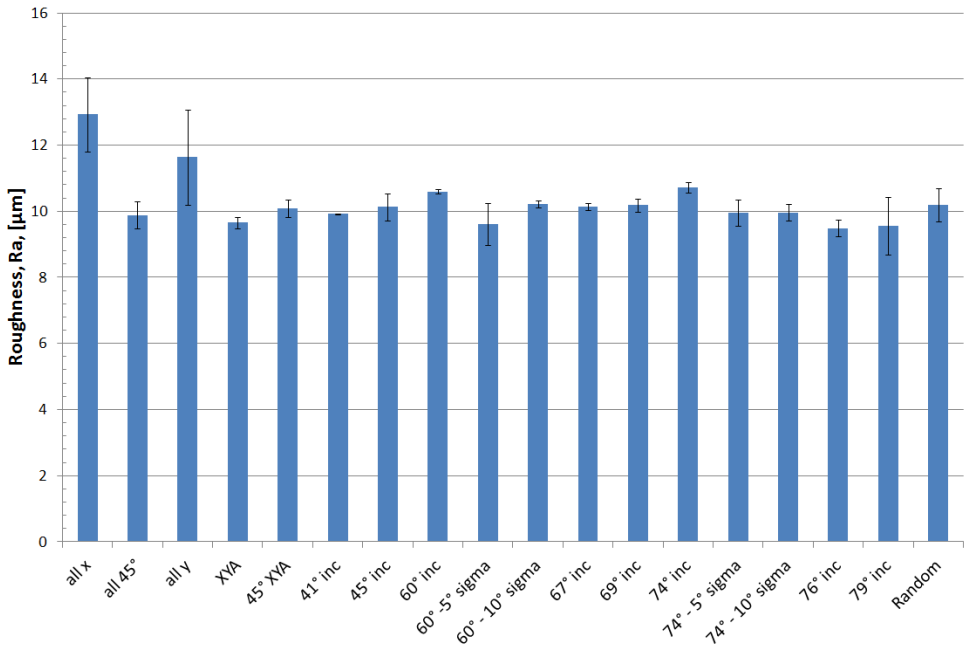

Figure 11 Top surface roughness of samples built with different angles of hatch rotation.

Tensile Strength Characteristics

The effect of hatch angle rotation on the strength of the components is shown (Figure 12) and it can be seen that there is little difference between any of the samples. The average yield stress was 488 MPa and the average ultimate tensile strength (UTS) was 593 MPa. The tensile strength properties are therefore not effected by variation to hatch vector rotation, at least for small area scans. The manufacture of the tensile test specimens aligned with the build axis of the system. This build orientation reduced residual stress manifestation in the tensile test specimens by minimising hatch vector lengths within the gauge cross section and therefore reduced the effects of constrained contraction.

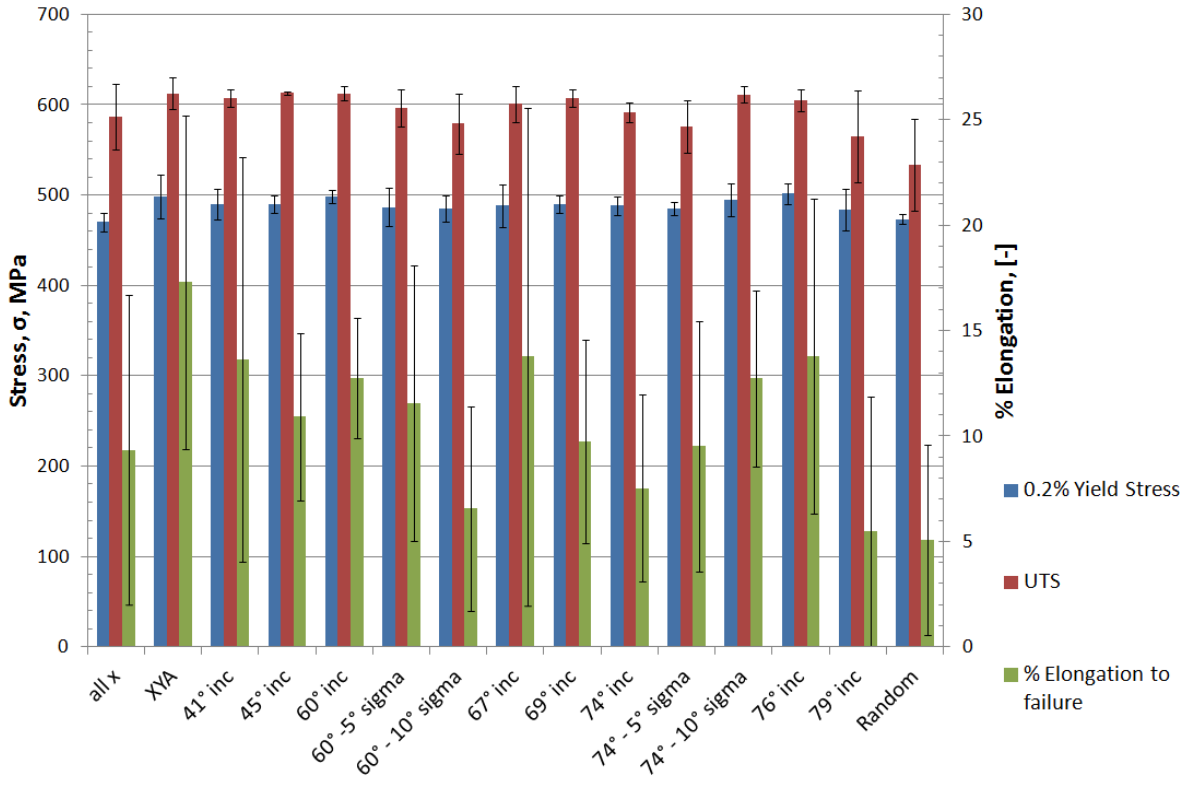

Figure 12 The effect of hatch rotation on the tensile properties of SLM parts.

The measured strengths of the SLM material are much greater than would be expected for CpTi as can be seen in Table 3. This is because of the differences in the microstructure of SLM parts compared with conventionally processed CpTi, this would have a direct effect on its mechanical properties. The grain size of a material is dependent on the thermal history of the part. In the case of SLM processing of CpTi the history is as follows; powder is initially heated by the laser until it melts and enters the melt pool with some of the previously formed solid beneath also being re-melted. As the laser moves further along the scan vector the material cools and begins to freeze and grains grow from the underlying microstructure. The witness lines of columnar β grains can be seen (Figure 13a) growing vertically up through the part. The temperature of the material then drops below the α-β transition temperature and α grains start to nucleate on the β boundaries, the high cooling rate causes a large number of nucleation events and so forms a very fine microstructure (Figure 13b). The change from the β phase to the α phase involves a change in lattice shape. Figure 13b shows that a shear transformation martensite structure is being created consisting of very fine needle like elongated grains due to the rapid transition from a body centred cubic to a hexagonal closed packed structure.

Table 3 Mechanical properties of grade 2 CpTi (Boyer et al. 1994) **and SLM CpTi.**

	CpTi (Grade 2)	SLM CpTi
0.2% Yield Strength (MPa)	275	488
Ultimate Tensile Strength (MPa)	345	593
Elongation to Failure (%)	20	10.6

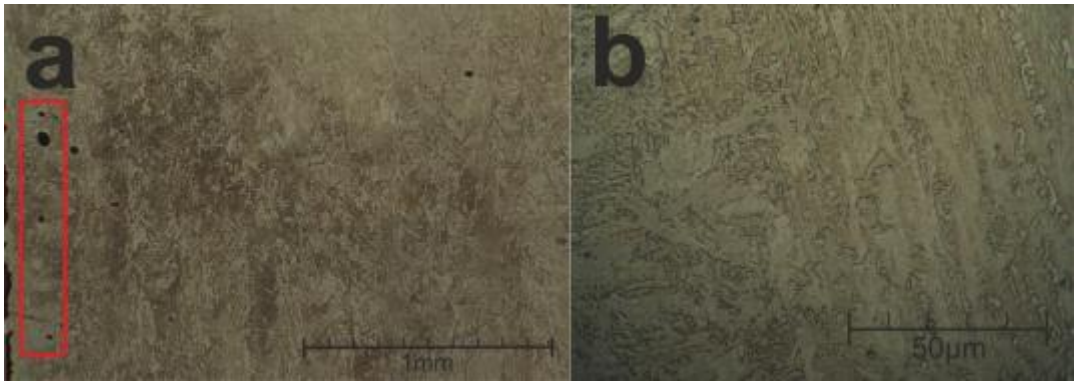

Figure 13 Side profile of a solid SLM part built with the parameters in Table 2 after polishing to 40nm and etching with HF taken at a) 100x magnification, the red box highlights the boundary scan porosity and b) 1000x magnification.

The elongation to failure results are less consistent with the maximum elongation to failure recorded at 29% and the minimum at least than 1%, so creating a large standard deviation. This was likely due to sub-surface porosity and, to a much lesser extent, surface finish. Any defect which can lead to a localised stress increase will decrease the elongation to failure of a specimen as they act as a crack initiation points. The poor surface finish of additively manufactured parts, compared to a machined samples, increases the sample material's notch sensitivity. The excess surface roughness was removed by the surface rub down with 240 grit paper however this only removed approximately 50 µm from each of the surfaces. To fully remove the effect of the rough surfaces from the experiment, the surfaces would need to be machined, thereby removing large amounts of material. However the surface post-processing performed did not affect the UTS and yield properties of the bulk additively manufactured samples as these are not effected by localised defects. These bulk properties therefore agree with the high density results, in which > 99.5% density was achieved regardless of hatch rotation angle, which ignored the effects of sub-surface porosity by avoiding these non-optimised regions.

However large deviation in the elongation to failure is proposed to have been due to the sub-surface porosity of the samples. The external boundary of the part (Figure 13a) reveals there are a number of pores of the order of 50 µm between the boundary scan and the internal hatches. There are two possible causes for the porosity in this region either the hatch offset is too large or too small. If the offset is too large then the hatches will not join up with the boundary and will form a ring of porosity between the two. If the overlap it to great then the scanning of the boundary over the hatched part will ablate material and therefore leave a deficiency of material in this area thereby creating the pores. These pores will form crack initiation points and therefore reduce the elongation to failure. The boundary scan parameters had not been optimised for each hatch vector rotation and this gave rise to this sub-surface porosity. The bulk material/boundary parameters had been developed

simultaneously for the XY alternating strategy. As a result this strategy reported the largest average elongation to failure as seen in Figure 12.

Residual Stress Characteristics

The deflection of samples in both the X and Y directions after they were separated from the substrate is shown in Figure 14. Due to the designed aspect ratio of the part, deflections in the X direction are much greater than those in the Y and any difference in deflection is therefore due to the residual stress in the X direction. The unidirectional, all X and all Y, scan strategies give the largest and smallest deflections respectively and would indicate that the greatest residual stress is created parallel to the scanned vectors. This agrees with the work done by Kruth et al. (2010). This does however suggest that the main source of residual stress formation in SLM is due to constrained contraction. In TGM, the stress is formed normal to the scan vector direction. If this was the major cause of residual stress then the all Y scan strategy would have resulted in the largest magnitude deformations.

The XYA scanning strategy gives a deflection that lies between the extremes of the all X and all Y strategies. The deflection of this part is also not half way between the two unidirectional strategies, with the defection being closer to that of the lower all Y strategy. This would imply that the stress in the part cannot be calculated by the sum of the component layers. In this case the part is made up of half all X layers and half all Y. There must therefore be an interaction between the stresses in the successive layers of the part which reduces the total overall deflection of the part. One explanation for this would be due to the effects of the TGM, which are principally orientated normal to the scan vector. This mechanism adds residual stress because when the existing solidified material is heated it expands and fails in compression. For example in the deposition of an all Y layer on top of an all X, there is a large tensile stress in the X direction in the solid material directly below the layer being formed. The expansion in the material, caused by the formation of the new layer, must first relieve the tensile strain before any compressive strain occurs. This will reduce the magnitude of compressive strain above the yield point and result in a reduction in additional stress from the all y direction vectors.

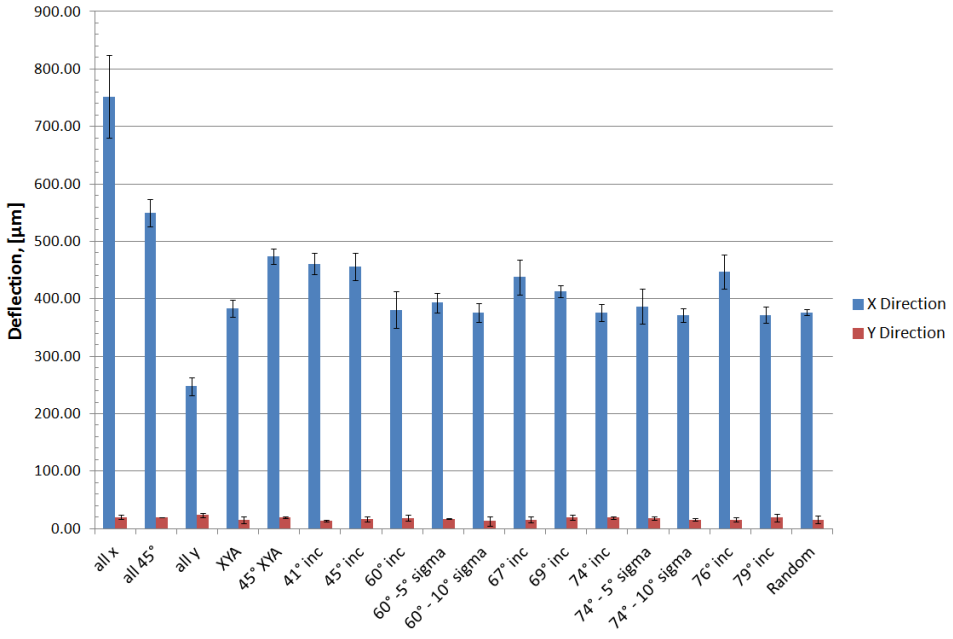

Figure 14 The effect of hatch angle rotation on deflection on parts on release from the substrate.

It can also be observed from the deflection results, that if the XYA strategy is rotated by 45° the measured deflection is larger implying that the stress in the part is not isotropic. The stress in the part is therefore still dependent on the orientation of the part. This factor should be considered for any strategy that repeats on itself quickly such as the parts built with a 60° increment. This also suggests that the absolute length of the each hatch vector has a large impact on resultant stress levels. Shorter hatch vectors have been found to reduce residual stresses (Kruth et al. 2012), and the results agree with the findings presented here that show the lowest part deformation was found for the all Y strategy.

The deflection for the XYA at 45° however is still similar to the other suggested hatch rotation angle strategies which have well distributed scan vectors as defined by the suitability measure. This test therefore gives some indication of the levels of stress within a part after manufacture. It also shows that the rotation of scan vectors does not lead to a drastic reduction in the levels of stress within a component as long as there is a rotation between layers. This rotation of scan vectors however may distribute the stresses in all directions better than the classic scan strategies which repeat quickly. However the significance of a 67° hatch rotation angle has not been proven from this research and has displayed no additional benefit over other rotation angles.

The deformations for the samples with Gaussian randomisations (Figure 14), are very similar to the corresponding non-randomised angles, implying that the levels of deformation, and therefore the levels of stress, are more dependent on the average angle of increment and are not affected by small deviations from this angle. The fact that the deflection for the full random sample is very similar to the other samples implies that the order in which the layers are added is less important than the distribution over a number of layers.

Conclusions

Modifications to the hatch angle appear to have very little effect on the density, surface finish or tensile properties of the material. The parameters developed for this study showed that near to full density could be attained with any of the hatching strategies, this agrees with the new simulation studies presented by Tang (2017). The sectioned parts also showed that there was a continuity of the structure throughout the height of the component. The grain structure of the material can be seen to span subsequent layers with no features indicating the different layers; this would eliminate the failure planes between layers. Therefore, no evidence has been gained regarding the optimum hatch angle increment for the production of SLM parts.

The effect of hatch angle rotation on residual stress is less clear. The residual stress was shown to be highly dependent on the direction in which the laser scans with the predominant stress being parallel to the direction of the scan vectors and therefore mainly derived from constrained contraction. The use of unidirectional scan vectors could be used to reduce the deflection in parts with slender aspect ratios. However, the stress is not being reduced but moved to a direction in which it has less effect. No hatch angle rotation, away from the 90° rotation strategies, displayed a significant drop in deflection measured. Therefore the hatch angle rotation of 67° promoted by Dimter (2011) and system manufacturers (Renishaw Plc 2017) has no specific benefits. However, as it has been shown that density and tensile strength will not be affected by alterations in hatch rotation angle, developers improving hatch strategies and part preparation software can alter the hatch angle intra-component

without detriment to strength or part porosity. This could lead to localised unidirectional hatch vectors in thin regions reducing part deformation due to residual stresses.

The findings of this study has shown that for certain geometries with a large aspect ratios, unidirectional scan vectors are beneficial in the reduction in resultant part deformation with the detriment of top surface roughness. For generalised shapes hatch rotation angles with a good Suitability Measure should be employed to mitigate directionality in part residual stresses reducing the likelihood of part failure. This has been shown by the increase in in part deformation produced using a 90° hatch angle rotation when the initial rotation angle was 45° with respect to the longest aspect of the multi-support deflection bridge.

References

Boyer, R., Welsch, G. & Collings, E.W., 1994. *Materials Properties Handbook: Titanium Alloys [electronic book]*, ASM International.

Dimter, M. et al., 2011. Method and Device for Manufacturing a Three-Dimensional Object.

Guan, K. et al., 2013. Effects of processing parameters on tensile properties of selective laser melted 304 stainless steel. *Materials & Design*, 50, pp.581–586.

Hague, R., Mansour, S. & Saleh, N., 2004. Material and design considerations for rapid manufacturing. *International Journal of Production Research*, 42(22), pp.4691–4708.

Kruth, J.-P. et al., 2012. Assessing and comparing influencing factors of residual stresses in selective laser melting using a novel analysis method. *Proceedings of the Institution of Mechanical Engineers, Part B: Journal of Engineering Manufacture*, 226(6), pp.980–991.

Kruth, J.-P. et al., 2010. Assessing Influencing Factors of Residual Stresses in SLM using a Novel Analysis Method. In *Proceedings of the 16th International Symposium on Electromachining*. pp. 531–537.

Kruth, J.-P. et al., 2004. Selective laser melting of iron-based powder. *Journal of Materials Processing Technology*, 149(1–3), pp.616–622.

Mercelis, P. & Kruth, J.-P., 2006. Residual stresses in selective laser sintering and selective laser melting. *RAPID PROTOTYPING JOURNAL*, 12(5), pp.254–265.

Mullen, L. et al., 2009. Selective Laser Melting: a regular unit cell approach for the manufacture of porous, titanium, bone in-growth constructs, suitable for orthopedic applications. *Journal of biomedical materials research. Part B, Applied biomaterials*, 89(2), pp.325–34.

Pohl, H. et al., 2001. Thermal stresses in direct metal laser sintering. In *Proceedings of the SFF Symposium*. pp. 366–372.

Renishaw Plc, 2017. Design for metal AM - a beginner's guide. Available at: http://www.renishaw.com/en/design-for-metal-am-a-beginners-guide--42652 [Accessed August 31, 2017].

Shiomi, M. et al., 2004. Residual Stress within Metallic Model Made by Selective Laser Melting Process. *CIRP Annals - Manufacturing Technology*, 53(1), pp.195–198.

Tang, M., 2017. *Inclusions, Porosity, and Fatigue of AlSi10Mg Parts Produced by Selective Laser Melting*. Carnegie Mellon University.

Thijs, L. et al., 2010. A study of the microstructural evolution during selective laser melting of Ti–6Al–4V. *Acta Materialia*, 58(9), pp.3303–3312.

Thijs, L. et al., 2013. Strong morphological and crystallographic texture and resulting yield strength anisotropy in selective laser melted tantalum. *Acta Materialia*, 61(12), pp.4657–4668.

Vollersten, F., 1998. Forming, Sintering and Rapid Prototyping. In *Handbook of the EuroLaser Academy*. Chapman & Hall, pp. 357–453.

Withers, P.J. & Bhadeshia, H.K.D.H., 2001. Residual stress. Part 1 – Measurement techniques. *Materials Science and Technology*, 17(4), pp.355–365.